

Online Centralized Non-parametric Change-point Detection via Graph-based Likelihood-ratio Estimation

Alejandro de la Concha

Argyris Kalogeratos

Nicolas Vayatis

Centre Borelli, ENS Paris-Saclay,
Université Paris-Saclay, France`{name.surname}@ens-paris-saclay.fr`

Abstract

Consider each node of a graph to be generating a data stream that is synchronized and observed at near real-time. At a change-point τ , a change occurs at a subset of nodes C , which affects the probability distribution of their associated node streams. In this paper, we propose a novel kernel-based method to both detect τ and localize C , based on the direct estimation of the likelihood-ratio between the post-change and the pre-change distributions of the node streams. Our main working hypothesis is the smoothness of the likelihood-ratio estimates over the graph, i.e. connected nodes are expected to have similar likelihood-ratios. The quality of the proposed method is demonstrated on extensive experiments on synthetic scenarios.

1 Introduction

Change-point detection is a fundamental problem in real time-series analysis and various control tasks. Modern challenges include handling larger amounts of more complex data streams, a clear example of which is when those lie over a graph. For example, many real-world systems can be seen as a network in which each node generates a stream of data: a network of seismic stations studying different geological events, the content shared by users of a social network, stations in a railway network, banks in a financial system, etc. A change-point may signify an earthquake, a shift of users' interest, a disruption of a railway service, or an early sign of an economic crisis. In these examples, the graph structure provides a priori relevant information about how the streams relate with each other, and maybe also shape their behavior after a change takes place.

In this paper, we address a naturally arising question: how can we capitalize over the graph information in the online change-point detection task?

Related work. Online, or sequential, change-point detection methods assume the user sees a stream of data in near real-time, and aim to detect the moment τ of a change-point as soon as possible, while minimizing the false alarm rate (Tartakovsky et al., 2014; Tartakovsky, 2021; Xie et al., 2021). Classical online change-point detection methods, such as Shewhart Chart (Shewhart, 1925), CUSUM (Page, 1954), and Sriryaev-Roberts (Shiryaev, 1963), are based on the likelihood-ratio of the probability models related to the data streams before and after the change-point. For some parametric families, whose members admit probability density functions p_θ and $p_{\theta'}$ described by a set of parameters θ, θ' , the aforementioned methods assume they know these parameters and hence achieve an optimal trade-off between detection delay and false alarms (Tartakovsky, 2021; Xie et al., 2021). Nevertheless, the hypothesis of complete knowledge of p_θ and q_θ is very restrictive in practice, mainly since the user rarely knows what to expect as system behavior after a change-point.

In Nguyen et al. (2008), the authors identified situations where the ϕ -divergence estimation between two measures amounts to inferring the likelihood-ratio as an element of a functional space, which means doing so indirectly using data observations coming from p and the assumed q . That work motivated the development of non-parametric approaches for change-point detection based on approximations of the likelihood-ratio. The methods of this line of work have the advantage of being agnostic to both the probabilistic models generating the data stream and the characteristics of the possible change (Yamada et al., 2011; Kanamori et al., 2012; Aminikhanghahi and Cook, 2017).

Both parametric and non-parametric methods were first applied to monitor a single data stream, but there has been a growing interest in extending these techniques to multiple streams. The latter refers to the case where each of the streams is associated with one node of a graph. Intuitively, the graph structure may carry relevant information for the fast detection of change-points. For the parametric case, we can point to Zou and Veeravalli (2018); Zou et al. (2019) where the knowledge of the process generating the streams

is assumed, as well as that the expected change will affect a connected subset of nodes. For the non-parametric case, Ferrari and Richard (2020) proposed a method where the underlying graph has community structure, and a change may occur in only one community (cluster of nodes).

Contribution. In this paper, we present the Online Centralized Kernel- and Graph-based (OCKG) detection method, which is built upon a non-parametric likelihood-ratio estimation and the notion of graph smoothness. The latter concept formalizes the intuition that two nodes are expected to have a similar behavior before and after a change-point if they are connected. More precisely, our approach is built upon the graph-based likelihood-ratio estimation framework of (de la Concha et al., 2022). The OCKG method has the notable advantages that it is: i) non-parametric and hence requiring minimum hypotheses about the nature of the data generating process at each of the graph nodes, ii) more sensitive compared to methods that aggregate all data streams in one stream, thanks to the integration of the graph structure, iii) more accurate in localizing the affected nodes, when compared with similar methods (e.g. Ferrari and Richard (2020)).

2 Background and problem statement

General notations. Let a_i be the i -th entry of a vector a ; when the vector is itself indexed by an index j , then we refer to its i -th entry by $a_{j,i}$. Similarly, A_{ij} is the entry at the i -th row and j -th column of a matrix A . $e_{\max}(A)$ denotes the maximum eigenvalue of A . $\mathbf{1}_M$ represents the vector with M ones (resp. $\mathbf{0}_M$), and \mathbb{I}_M is the $M \times M$ identity matrix. We denote by $G = (V, E, W)$ a positive weighted and undirected graph, where V is the set of vertices, E the set of edges, and $W \in \mathbb{R}^{N \times N}$ its adjacency matrix. The graph has no self-loops, i.e. $W_{uu} = 0, \forall u \in V$. The degree of v is $d_v = \sum_{u \in \text{ng}(v)} W_{uv}$, where $u \in \text{ng}(v)$ indicates that u is a neighbor of v . The degree of node v is indicated by d_v ; $\text{ng}(v) = \{u : W_{uv} \neq 0\}$ is the set of all the neighbors of v . With these elements, we can define the combinatorial Laplacian operator associated with G as $\mathcal{L} = \text{diag}((d_v)_{v \in V}) - W$, where $\text{diag}(\cdot)$ is a diagonal matrix with the elements of the input vector in its diagonal. Finally, we will later find useful the notion of *graph function*, which is any function $\omega : V \rightarrow \mathbb{R}^d$ assigning a vector in \mathbb{R}^d to each node of a graph. When $d = 1$, ω defines a *graph signal* (Shuman et al., 2013).

ϕ -divergences and likelihood-ratio. ϕ -divergences provide a way to measure the similarity between two probability measures. When both measures admit a pdf, let those be p and q , respectively, in terms of the Lebesgue measure, then ϕ -divergence is defined as: $I_\phi(p, q) = \int p(x) \phi\left(\frac{q(x)}{p(x)}\right) dx$, for $x \in \mathcal{X}$. where $\phi : \mathbb{R} \rightarrow \mathbb{R}$ is a convex and semi-continuous real function such that $\phi(1) = 0$ (Csiszár,

1967). Notably, for $\chi \in \mathbb{R}$, when $\phi(\chi) = \log(\chi)$ we recover the well-known Kullback–Leibler’s (KL-divergence) (Kullback, 1959) which is omnipresent in most optimality theorems for online change-point detection methods (Tartakovsky et al., 2014; Tartakovsky, 2021; Xie et al., 2021). When $\phi(\chi) = \frac{(\chi-1)^2}{2}$, we identify the Pearson’s PE-divergence (Pearson, 1900).

The quantity $r(x) = \frac{q(x)}{p(x)}$ is called *likelihood-ratio*, and is central in the computation of any ϕ -divergence. As we will see in Sec. 3.1, we can translate the approximation of a PE-divergence between p and q to a likelihood-ratio estimation problem. In practice, though, r may be an unbounded function, challenging non-parametric methods that may fail to converge. For this reason, a known workaround is to replace p by $p^\alpha(x) = (1-\alpha)p(x) + \alpha q(x)$, and use instead the α -relative likelihood-ratio function (Yamada et al., 2011):

$$r^\alpha(x) = \frac{q(x)}{(1-\alpha)p(x) + \alpha q(x)} = \frac{q(x)}{p^\alpha(x)} \leq \frac{1}{\alpha}, \quad (1)$$

for any $0 \leq \alpha < 1$, $x \in \mathcal{X}$.

Proposed setting and problem statement. Let us suppose we observe N synchronous data streams, each generated by a node of a connected graph G . Let $x_{v,t}$ be the observation at node v at time t . We suppose that, $\forall v \in V$ and $t \in \{1, \dots\}$, $x_{v,t} \in \mathcal{X}$ belongs to the same input space $\mathcal{X} \subset \mathbb{R}^d$. Furthermore, the observations are independent in time, which is a standard hypothesis in kernel-based change-point detection literature (Arlot et al., 2019; Li et al., 2019; Harchaoui et al., 2008; Bouchikhi et al., 2019).

Consider as change-point the timestamp τ at which the distribution associated with the streams observed at nodes belonging to a set C , changes:

$$\begin{cases} t < \tau & x_{v,t} \sim p_v; \\ t \geq \tau & x_{v,t} \sim q_v; \end{cases} \quad (2)$$

where $p_v \neq q_v$ if $v \in C$, otherwise $p_v = q_v$. We consider all p_v, q_v, C, τ to be unknown. Moreover, we expect C to depend on the graph structure. A simple example with signals $\mathcal{X} \subset \mathbb{R}^2$ at each node, is shown in Fig. 1.

For each node v , let us define the sample of n consecutive observations, indexed by t , to be the set:

$$\mathcal{X}_{v,t} = [x_{v,t-n}, x_{v,t-(n-1)}, \dots, x_{v,t-1}]. \quad (3)$$

Our method aims to compare the two adjacent samples, $\mathcal{X}_{v,t}$ and $\mathcal{X}_{v,t+n}$, for each node. More precisely, we learn jointly the N relative likelihood-ratios $r^\alpha(\cdot) = (r_1^\alpha(\cdot), \dots, r_N^\alpha(\cdot))^T \in \mathbb{R}^N$ (see Eq. 1) and use them to design a score that indicates whether $\mathcal{X}_{v,t}$ and $\mathcal{X}_{v,t+n}$ follow the same distribution.

In the text, we call *null hypothesis* (H_{null}) the case with no change, i.e. when $p_v = p'_v, \forall v \in V$, which opposes the *alternative hypothesis* (H_{alt}) where a change does exist.

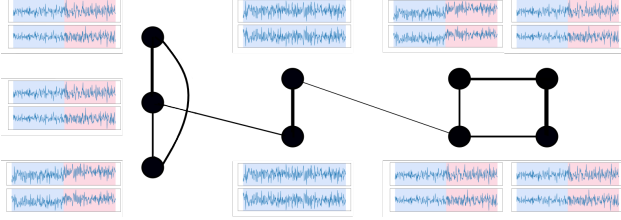


Figure 1: Example of two-dimensional data streams observed over the nodes of a weighted graph. A change occurs in a subset of nodes, and the change-point is at the moment when the color changes in the respective time-series. Left nodes: their change-point is associated with a shift in the covariance matrix. Right nodes: they experience a shift in the mean of their streams.

3 Problem formulation and solution

The proposed Online Centralized Kernel- and Graph-based (OCKG) change-point detection method capitalizes over the connection between the approximation of the Pearson’s PE-divergence and the likelihood-ratio estimation. This technique allows us to compare the samples $\mathcal{X}_{v,t}$ and $\mathcal{X}_{v,t+n}$. By definition, the PE-divergence is a non-symmetric similarity measure, i.e. generally $PE(p,q) \neq PE(q,p)$. For this reason, we generate approximations for both quantities.

In summary, the OCKG method comprises three main tasks to which the next subsections are devoted:

1. **Estimation:** When a new observation arrives at time t , we estimate the vector of relative likelihood-ratios $r^{\vec{\alpha}}_t(\cdot) = (r^{\vec{\alpha}}_{1,t}(\cdot), \dots, r^{\vec{\alpha}}_{N,t}(\cdot))$, between the samples of observations $\mathcal{X}_t, \mathcal{X}_{t+n}$, and for the reverse sample order $r^{\vec{\alpha}}_t(\cdot)$ with samples $\mathcal{X}_{t+n}, \mathcal{X}_t$.
2. **Detection:** The estimated likelihood-ratios $r^{\vec{\alpha}}_t(\cdot)$ and $\tilde{r}^{\vec{\alpha}}_t(\cdot)$ are used to approximate the respective PE-divergences, $\hat{PE}_v^\alpha(\mathcal{X}_t, \mathcal{X}_{t+n})$ and $\hat{PE}_v^\alpha(\mathcal{X}_{t+n}, \mathcal{X}_t)$. Then, we define node scores, $\{S_v\}_{v \in V}$, based on the latter approximations. Finally, the node scores are aggregated into a global score indicating whether a change has occurred in the system.
3. **Identification:** Once a change-point is spotted, we use the node scores $\{S_v\}_{v \in V}$ to identify the nodes at which the change occurred, thus belonging to C .

3.1 Estimation

The OCKG method relies on the quantification of the difference between the probability models pdfs p_v and q_v based just on two adjacent n -sized samples $\mathcal{X}_{v,t}$ and $\mathcal{X}_{v,t+n}$. This is done by exploiting the interplay between the ϕ -divergence and the likelihood-ratios; more precisely, let us quote the following lemma (Lemma 2 in Nguyen et al. (2008)) referring to the ϕ -divergence of p_v and q_v :

Lemma 1. For any class of functions \mathcal{F} mapping from \mathcal{X} to \mathbb{R} , we have the lower bound for the ϕ -divergence:

$$I_\phi(p, q) \geq \sup_{f \in \mathcal{F}} \int [f(x)q(x)dx - \phi^*(f(x))p(x)]. \quad (4)$$

Equality holds if and only if the subdifferential $\partial\phi(\frac{q(x)}{p(x)})$ contains an element of \mathcal{F} , where ϕ^* is the conjugate dual function of ϕ , i.e. $\phi^*(v) = \sup_{u \in \mathbb{R}} [uv - \phi(u)]$.

When we fix $\psi(\chi) = \frac{(\chi-1)^2}{2}$, we recover the PE-divergence, and according to the Lemma 1 we write:

$$PE(p, q) = \int r(x)q(x)dx - \int \frac{r^2(x)}{2}p(x)dx - \frac{1}{2}, \quad (5)$$

where $r(x) = \frac{q(x)}{p(x)}$ is the likelihood-ratio. We can use Eq. 5 to translate the approximation of the PE-divergence between p and q to a likelihood-ratio estimation problem. As mentioned in Sec. 2, in practice r can be unbounded and prevent the convergence of non-parametric methods. We thus use instead the α -relative likelihood-ratio of Eq. 1.

Our graph-related objective is to estimate jointly the N node-level α -relative likelihood-ratio functions $r_v^\alpha(x)$, $v \in V$, each one being associated with the node v ’s pdfs q_v and q'_v . Our two main hypotheses are that: i) each $r_v^\alpha(x)$ is an element of a Reproducing Kernel Hilbert Space (RKHS), and that ii) the graph signal $r^\alpha(x) = (r_1^\alpha(x), \dots, r_N^\alpha(x))$ is expected to be also smooth after the change-point. Notice that, when $p = q$, $r^\alpha(x)$ is the constant vector $\mathbf{1}_M$, which is obviously a perfectly smooth graph signal.

3.1.1 Cost function

Let us introduce the RKHS \mathbb{H} equipped with a reproducing kernel $K : \mathcal{X} \times \mathcal{X} \rightarrow \mathbb{R}$, with the associated inner-product $\langle \cdot, \cdot \rangle_{\mathbb{H}}$ and feature map $\phi(\cdot) : \mathcal{X} \rightarrow \mathbb{H}$. Let $f_v(\cdot)$ be the function approximating $r_v^\alpha(\cdot) = \frac{q_v(\cdot)}{(1-\alpha)p_v(\cdot) + \alpha q_v(\cdot)} = \frac{q_v(\cdot)}{p_v^\alpha(\cdot)}$; we suppose $f_v(\cdot)$ is a linear model of the form $f_v(x) = \langle \theta_v, \phi(x) \rangle_{\mathbb{H}}$, where $\theta_v \in \mathbb{H}$. In practice, we will have access to L elements of a global dictionary $D = \{x_1, \dots, x_L\}$ shared by all nodes. Therefore, the vectorized form of the kernel feature map is $\phi(x) = (K(x, x_1), \dots, K(x, x_L))$, $\forall x \in \mathcal{X}$ and $\theta_v \in \mathbb{R}^L$. The linear model can now be expressed as:

$$f_v(x) = \sum_{l=1}^L \theta_{v,l} K(x, x_l). \quad (6)$$

And by definition it holds:

$$|f_v(x) - f_u(x)| \leq \|\phi\|_{\mathbb{H}} \|\theta_u - \theta_v\|_{\mathbb{H}}. \quad (7)$$

If the norm of the feature map $\|\phi\|_{\mathbb{H}}$ is bounded for all x , then we can guarantee that $f_v(x)$ and $f_u(x)$ are close if the parameters θ_u and θ_v are close as well. This means we can induce smoothness to the graph signal $f(\cdot) =$

$(f_1(\cdot), \dots, f_N(\cdot))$ in terms of their parameters $\{\theta_v\}_{v \in V}$. We will denote the concatenation of the parameters of interest as $\Theta = (\theta_1, \dots, \theta_N)$.

With these elements, we can define the optimization Problem 8 that is made of two components: the first term is a least square cost function aiming to approximate the relative likelihood-ratio at the node-level; the second term induces smoothness to the functions f_u and f_v by making their associated parameters, θ_u and θ_v of any two connected nodes u and v , to be similar, while controlling the risk of overfitting via the penalization term $\|\theta_u\|^2$ (Sheldon, 2008):

$$\begin{aligned} & \min_{\Theta \in \mathbb{R}^{NL}} \frac{1}{N} \sum_{v \in V} \frac{\mathbb{E}_{p_v^\alpha(x)}[(r_v^\alpha(x) - f_v(x))^2]}{2} \\ & \quad + \frac{\lambda}{2} \sum_{u,v \in V} W_{uv} \|\theta_u - \theta_v\|^2 + \frac{\lambda\gamma}{2} \sum_{v \in V} \|\theta_v\|^2 = \\ & \min_{\Theta \in \mathbb{R}^{NL}} \frac{1}{N} \sum_{v \in V} \left(\frac{\mathbb{E}_{p_v^\alpha(x)}[(\theta_v, \phi(x))^2]}{2} - \mathbb{E}_{q_v(x)}[\langle \theta_v, \phi(x) \rangle] \right) \\ & \quad + \frac{\lambda}{2} \sum_{u,v \in V} W_{uv} \|\theta_u - \theta_v\|^2 + \frac{\lambda\gamma}{2} \sum_{v \in V} \|\theta_v\|^2 + \Xi. \end{aligned} \quad (8)$$

The equality between the two expressions comes from the development of the square in the first term, and the fact $E_{q_v^\alpha}[(g(x)r_v^\alpha(x))] = E_{q_v'}[g(x)]$. Note that $\gamma, \lambda > 0$ are penalization constants, and Ξ is a term we can ignore since it does not depend on Θ .

Let us suppose that, at time t , for each node v we have access to observations coming from the two probabilistic models described by q_v and q_v' , which we respectively denote by \mathcal{X}_v and \mathcal{X}'_v . We define the elements:

$$\begin{aligned} H_{v,t} &= \frac{1}{n} \sum_{x \in \mathcal{X}_v} \phi(x)\phi(x)^\top, & H'_{v,t} &= \frac{1}{n} \sum_{x \in \mathcal{X}'_v} \phi(x)\phi(x)^\top, \\ h'_{v,t} &= \frac{1}{n} \sum_{x \in \mathcal{X}'_v} \phi(x). \end{aligned} \quad (9)$$

Then, by rewriting Problem 8 in terms of empirical expectations, we get:

$$\begin{aligned} & \min_{\Theta \in \mathbb{R}^{NL}} \frac{1}{N} \sum_{v \in V} \left((1-\alpha) \frac{\theta_v^\top H_{v,t} \theta_v}{2} + \alpha \frac{\theta_v^\top H'_{v,t} \theta_v}{2} - h'_{v,t} \theta_v \right) \\ & \quad + \frac{\lambda}{4} \sum_{u,v \in V} W_{uv} \|\theta_u - \theta_v\|^2 + \frac{\lambda\gamma}{2} \sum_{v \in V} \|\theta_v\|^2 \\ & = \frac{1}{N} \left(\sum_{v \in V} \ell_{v,t}(\theta_v) \right) + \frac{\lambda}{2} \Theta^\top ([\mathcal{L} + \gamma \mathbb{I}_N] \otimes \mathbb{I}_L) \Theta, \end{aligned} \quad (10)$$

where $\ell_{v,t}(\theta_v) = (1-\alpha) \frac{\theta_v^\top H_{v,t} \theta_v}{2} + \alpha \frac{\theta_v^\top H'_{v,t} \theta_v}{2} - h'_{v,t} \theta_v$, and \otimes is the Kronecker product between two matrices.

Let us call $\hat{\Theta}_t = (\hat{\theta}_1^\top, \hat{\theta}_2^\top, \dots, \hat{\theta}_N^\top)$ the solution of Problem 8, and $\{\hat{f}_{v,t}(\cdot)\}_{v \in V}$ the estimated relative likelihood-ratio. Then we can approximate the PE-divergence $PE(q_v^\alpha, q_v)$ using an empirical approximation of Eq. 5 and the estimation $\hat{f}_{v,t}(\cdot)$:

$$\begin{aligned} \hat{PE}_v^\alpha(\mathcal{X}_{v,t}, \mathcal{X}'_{v,t}) &= \sum_{x' \in \mathcal{X}'_v} \frac{\hat{f}_{v,t}(x)}{n} - \frac{(1-\alpha)}{2} \left(\sum_{x \in \mathcal{X}_v} \frac{\hat{f}_{v,t}(x)^2}{n} \right) \\ & \quad - \frac{\alpha}{2} \left(\sum_{x' \in \mathcal{X}'_v} \frac{\hat{f}_{v,t}(x')^2}{n} \right) - \frac{1}{2} \\ & = - \left((1-\alpha) \frac{\hat{\theta}_{v,t}^\top H_{v,t} \hat{\theta}_{v,t}}{2} + \alpha \frac{\hat{\theta}_{v,t}^\top H'_{v,t} \hat{\theta}_{v,t}}{2} - h'_{v,t} \hat{\theta}_{v,t} \right) - \frac{1}{2} \\ & = -\ell_{v,t}(\hat{\theta}_{v,t}) - \frac{1}{2}. \end{aligned} \quad (11)$$

The lack of symmetry of PE-divergence is relevant in the change-point detection task, since at every time t we need to compare the two samples associated with the probabilistic models described by $\{p_v\}_{v \in V}$ and $\{p'_v\}_{v \in V}$ respectively. Depending on which pdf is taken as numerator in $r_v^\alpha(\cdot)$, the associated PE-divergence may vary its sensibility to detect change-points. For this reason, we estimate two parameters $\hat{\Theta}_t$ and $\hat{\Theta}_t$ to approximate $\hat{PE}_v^\alpha(\mathcal{X}_{v,t}, \mathcal{X}_{v,t+n})$ and $\hat{PE}_v^\alpha(\mathcal{X}_{v,t+n}, \mathcal{X}_{v,t})$, respectively.

3.1.2 Optimization procedure

$$\begin{aligned} H_t &= \text{Block}(H_{1,t}, \dots, H_{N,t}) \in \mathbb{R}^{NL \times NL}, \\ H'_t &= \text{Block}(H'_{1,t}, \dots, H'_{N,t}) \in \mathbb{R}^{NL \times NL}, \\ h'_t &= (h'_{1,t}, \dots, h'_{N,t}) \in \mathbb{R}^{NL}. \end{aligned} \quad (12)$$

With these terms, we can easily verify that the optimization Problem 10 is in fact a Quadratic problem:

$$\begin{aligned} \min_{\Theta \in \mathbb{R}^{NL}} \Phi_t(\Theta) &= \min_{\Theta \in \mathbb{R}^{NL}} \frac{\Theta^\top (A_t) \Theta}{2} - \Theta^\top b_t \\ &= \min_{\Theta \in \mathbb{R}^{NL}} \frac{\Theta^\top \left(\frac{1-\alpha}{N} H_t + \frac{\alpha}{N} H'_t + ([\mathcal{L} + \gamma \mathbb{I}_N] \otimes \mathbb{I}_L) \right) \Theta}{2} - \Theta^\top h'_t. \end{aligned} \quad (13)$$

Note that $A_t = \frac{1-\alpha}{N} H_t + \frac{\alpha}{N} H'_t + [\mathcal{L} + \gamma \mathbb{I}_N] \otimes \mathbb{I}_L$ defines a positive definite matrix. Then, at every time t we could obtain a closed-form solution $\hat{\Theta}_t = A_t^{-1} b_t$. Nevertheless, in real applications, the size of the graph and the dictionary may cause this matrix inversion to be infeasible. For this reason, we propose to solve the problem via the Cyclic Block Coordinate Gradient Descent (CBCGD) method (Beck and Tetrushvili, 2013; Li et al., 2018).

In our formulation, each block of variables is associated with a node v , thus it contains θ_v . Before applying CBCGD, we need to define a fixed order for update of the variables. Let $\theta_{<v}$ be the set of variables that were updated before v , and $\theta_{\geq v}$ be the complement of that set. Then, the

i -th update of the parameter $\hat{\theta}_{v,t}$ is performed according to the schema:

$$\hat{\theta}_{v,t}^{(i)} = \frac{1}{\eta_{v,t} + \lambda\gamma} \left[\underbrace{\eta_{v,t} \hat{\theta}_{v,t}^{(i-1)}}_{\text{component depending on node } v} - \underbrace{\left(\frac{(1-\alpha)H_{v,t} + \alpha H'_{v,t}}{N} \hat{\theta}_{v,t}^{(i-1)} - \frac{h'_{v,t}}{N} \right)}_{\text{component depending on the graph}} - \lambda \left(d_v \hat{\theta}_{v,t}^{(i-1)} - \sum_{u \in \text{ng}(v)} W_{uv} (\hat{\theta}_{u,t}^{(i)} \mathbf{1}_{u < v} + \hat{\theta}_{u,t}^{(i-1)} \mathbf{1}_{u \geq v}) \right) \right]. \quad (14)$$

An important point to highlight is the behavior of this schema when the graph structure is ignored. If we set $W = \mathbf{0}_{M \times M}$, we recover a gradient descent algorithm running independently for each node (i.e. ignoring the graph). This variant is called Pool in the experiments of Sec. 4.

Notice that when no change has occurred, we expect the problem instances Φ_t and Φ_{t+1} to be similar. Thus, in this case, we can use the solution $\hat{\Theta}_{t-1}$ to initialize the problem for solving Φ_{t+1} . More over, we can prove that the fact our problem is quadratic the number of cycles required to generate a new estimate $\hat{\Theta}_t$ from a new observation arriving to all the nodes and the previous estimate $\hat{\Theta}_{t-1}$ scales nicely even in big graphs. This statement can be found in Appendix A as Theorem 1. The conclusion of the theorem is, first, that the number of cycles between points from time t to time $t+1$ remain manageable, due to the efficient initialization of Φ_{t+1} with Θ_{t-1} (as explained earlier); second, the graph size impacts the optimization at a rate of $O(\log^2(N))$, which is manageable for many real graphs.

3.2 Detection and identification

A well-known property of $PE(p, q) \geq 0$, is that it becomes zero if and only if $p = q$, which makes it a good candidate as a score to validate whether a change exists (Kawahara and Sugiyama, 2012). Then, the definition of a node-level score comes naturally:

$$S_{v,t} = \max\{\hat{PE}_v^\alpha(\mathcal{X}_{v,t}, \mathcal{X}_{v,t+n}) + \hat{PE}_v^\alpha(\mathcal{X}_{v,t}, \mathcal{X}_{v,t+n}), 0\}. \quad (15)$$

The maximum is taken as the approximations can be negative. Next we define the global score $S_t = \sum_{v \in V} S_{v,t}$, which triggers a global alarm when $S_t \geq \eta$, where $\eta > 0$ is a threshold parameter fixed by the user. The moment τ at which this global alarm fires, is also the estimated occurrence time of the associated change-point.

Once a change-point has been detected, we need to identify the affected nodes of the subset C . We select the nodes that satisfy $S_{v,t} > \eta_v$, where $\{\eta_v\}_{v \in V}$ is a set of positive constants given by the user.

The detailed pseudocode of OCKG is described in Alg. 1.

Notice that by design, we expect $\hat{PE}_v(\cdot, \cdot)$ to achieve its maximum value when it compares $\mathcal{X}_{v,\tau}$ and $\mathcal{X}_{v,\tau+n}$, which means there is always a lag of size n (observations) in the detection of τ . We desire n to be as small as possible, yet guarantying a good identification of the nodes of interest. We further discuss this point in the experiments of Sec. 4.

3.3 Further implementation details

Dictionary. In the previous section, we have made the implicit hypothesis that we have access to a predefined dictionary D and that it remains stable through time. This can be hard in practice, especially since in a change-point detection task we expect that at some point the observations will start being different to what will have been seen till then. Therefore, it is important to update the dictionary with new observations in an online manner, in order to improve the quality of the estimators $\hat{f}_{v,t}(\cdot)$. More specifically, we follow the approach that was suggested by Richard et al. (2009) in the context of online prediction for time-series, where new observations get included into a dictionary, while controlling its size and the sparse representation of the datapoints. This is achieved by the *coherence* measure that quantifies the redundancy between the dictionary elements as being linearly dependent. If this is smaller than a given threshold μ_0 , the new datapoint is added into the dictionary. After reaching a maximum dictionary size L , we delete the datapoint with the highest coherence (i.e. highest redundancy) each time we insert a new element to the dictionary.

Hyperparameter Selection. An important question that remains to be answered is how to select the hyperparameters associated with the kernel K , and the penalization constants λ and γ . As in previous works in non-parametric ϕ -divergence estimation, we use a cross-validation strategy (Sugiyama et al., 2007, 2011; Yamada et al., 2011). This tries to minimize the sum of the losses $\frac{1}{N} \sum_{v \in V} \ell_{v,t}(\theta_v)$, which is equivalent to maximizing the mean node-level PE-divergences. The hyperparameter selection procedure is described by Alg. 2 included in Appendix B. In order to keep the computational cost reasonable, we recommend estimating the right hyperparameters just once in each direction. In the experiments, we applied this approach using a set of observations that had no change-points.

The value of α is important for the stability of the algorithm. In the univariate case, it has been shown that the convergence rates of the cost function inspired by the Pearson Divergence depends on $\|r_\alpha\|_\infty$ Yamada et al. (2011). This means that a higher α value is expected to improve the convergence with respect to the number of observations, but on the other hand it will make harder to identify whether p and q differ. The role of α value is also investigated in our experiments.

Algorithm 1 The OCKG detector

1: **Input:**
 $\alpha \in [0, 1]$: parameter of the relative likelihood-ratio (Eq. 1);
 n : the size of the sample to use;
 D_1, D_2 : precomputed dictionaries, with L_1 and L_2 elements, respectively;
 $(\sigma_1^*, \lambda_1^*, \gamma_1^*), (\sigma_2^*, \lambda_2^*, \gamma_2^*)$: optimal hyperparameters (Alg. 2);
 μ_0, L : coherence threshold controlling the dictionary updates, and the maximum dictionary size;
 tol : tolerated relative error for the optimization process;
 $\eta, \{\eta_v\}$: threshold to raise a global alarm, η_v threshold to raise an alarm at node v .

2: **Output:** $\hat{\tau}$: the detection time of the change;
 \hat{C} : the set of nodes where the change is observed.

■ **Initialization of parameters**

3: $\tilde{\Theta}_n^{(0)} = \tilde{\Theta}_n^{(0)} = \mathbf{0}_{LN}$

■ **Online estimation and detection**

4: **for** $t \in \{n, \dots\}$ **do**
 5: **for** $v \in \{1, \dots, N\}$ **do**
 6: Observe $x_{v,t+n-1}$ and update the sliding windows $\mathcal{X}_t, \mathcal{X}_{t+n}$ (Eq. 3)
 □ **Dictionary update**
 if $\max_{l \in \{1, \dots, L_1\}} k(x_{v,l}, x_{v,t+n-1}) \leq \mu_0$ **then**
 8: Add $x_{v,t+n-1}$ to the dictionary D_1
 9: **if** the maximum dictionary size is reached, delete the datapoint with the highest coherence
 end if
 10: **end if**
 11: □ **Parameters update**
 12: Define $\vartheta_v = [\theta_{v,t-1}^\top, \mathbf{0}_{d_1}]$, (d_1 is the number of new elements added to the dictionary)
 13: Initialize $\tilde{\theta}_{v,t-1}^{(0)} = \vartheta_v$
 14: Fix $\mathcal{X} = \mathcal{X}_t$ and $\mathcal{X}' = \mathcal{X}_{t+n}$
 15: **for** $v \in \{1, \dots, N\}$ **do**
 16: Compute the quantities H_v, H'_v, h'_v . (see Eq. 9)
 17: Fix $\eta_{v,t} = e_{\max} \left(\frac{(1-\alpha)H_{v,t} + \alpha H'_{v,t}}{N} + \lambda d_v \mathbb{I}_{L_1} \right)$
 18: **end for**
 19: **while** $\left\| \tilde{\Theta}_t^{(i)} - \tilde{\Theta}_t^{(i-1)} \right\| > \epsilon$ **do**
 20: **for** $v \in \{1, \dots, N\}$ **do**
 21: Update $\tilde{\theta}_v^{(i)}$ (see Eq. 14)
 22: **end for**
 23: **end while**
 24: **for** $v \in \{1, \dots, N\}$ **do**
 25: Estimate $\hat{P}E_v^\alpha(\mathcal{X}_v, \mathcal{X}'_v)$ (see Eq. 11)
 26: **end for**
 27: Fix $\mathcal{X} = \mathcal{X}_{t+n}$ and $\mathcal{X}' = \mathcal{X}_t$
 28: Repeat steps 6–22 to compute $\tilde{\Theta}_t$ and $\hat{P}E_v^\alpha(\mathcal{X}'_{v,t}, \mathcal{X}_{v,t})$
 29: □ **Online detection and Identification**
 30: Compute the node scores $S_{v,t}$ (see Eq. 15)
 31: Compute the global score $S_t = \sum_{v \in V} S_{v,t}$
 32: **if** $S_t > \eta$ **then**
 33: A change-point is detected at $\hat{\tau} = t$
 34: **if** $S_{v,t} > \eta_v$ **then**
 35: Add v to \hat{C}
 36: **end if**
 37: **end if**
 38: **end for**
 39: **Return** $\hat{\tau}$ and \hat{C}

4 Experiments

Competitors. In this section we compare the performance of the OCKG detector against two other alternatives that are based on non-parametric estimation. We refer to those methods as Nougat and Pool in the reported results.

Nougat is a non-parametric method aiming to detect a change in a cluster of graph nodes (Ferrari and Richard, 2020; Ferrari et al., 2021). It estimates the node-level likelihood-ratio via kernel methods and a stochastic gradient descent. At every time t a single step of stochastic gradient descent is performed, and the updated function is then evaluated at time $t+1$ with the new incoming observation. This is done independent for each of the nodes of the graph. The resulting evaluation of the estimated function is used to construct a graph signal. Finally, Nougat filters the signal with the Graph Fourier Scan Statistic (GFSS), a graph-based statistical test that has been used for detecting nodes with anomalous activity in a graph (Sharpnack et al., 2016). The score for node v is the absolute value of the v -th entry of the filtered signal, and the global score is the norm of this vector.

Pool is a variant of the proposed OCKG that ignores the graph structure, i.e. when we set $W = \mathbf{0}_{M \times M}$, and thus serves a baseline for investigating the benefits of using the graph. In this configuration, there is a global dictionary available for all the nodes, which is updated as observations become available, and the updates of the node parameters θ_v are carried out independently for each of the nodes. This detector can be seen as a RULSIF-based adaptation (Sugiyama et al., 2007). RULSIF is a state-of-the-art approach that has proved to be superior empirically and theoretically, when compared with other likelihood-ratio based methods (Kawahara and Sugiyama, 2012).

Setup. For all the detectors, we focus on the Gaussian kernel, which means that among the hyperparameters to optimize there are the associated σ parameters of this type of kernel. Then, for each compared detector, there is a different set of regularization parameters to tune. For OCKG the regularization terms are λ and γ , while just γ for Pool and Nougat. For Pool and OCKG, we run the method described in Alg. 2 in a set of observations of size $2n$ where there are no change-points. The same set of observations is used to build the initial dictionary according to the approach described in (Richard et al., 2009) with the coherence threshold parameter $\mu_0 = 0.1$. The same coherence threshold is used for the online updating of the dictionary.

For Nougat, the selection of the hyperparameters σ and λ is not easy, as this was left as an open question in the original papers presenting this approach. To overcome this limitation we run the same procedure that we apply to Pool, but using $\alpha = 0$, since Nougat in fact estimates the unregularized likelihood-ratios $r_v(x) - 1 = \frac{q_v(x)}{p_v(x)} - 1$. On the other

hand, for the dictionary building strategy, Nougat referred to (Ferrari et al., 2021) that uses a similar approach as the one we use for OCKG and Pool. There are two more parameters to be fixed in Nougat: the learning rate η_v of the gradient descent, and a parameter associated with the GFSS and the spectrum of the graph. For the learning rate, we fix $\eta_v = \frac{1}{10e_{\max}((H_{v,0} + \gamma \mathbb{1}_L))}$ inspired by the convergence guarantees provided in (Ferrari et al., 2021), where $H_{v,0}$ is build with n observations coming from $p_v(\cdot)$ (Eq. 9). Finally, we pick the smallest non-zero eigenvalue of the Laplacian as the tuning parameter of the GFSS filter, which also provided the best results.

In order to select the width σ for the Gaussian kernel, we first compute $\{\sigma_v\}_{v \in V}$ for each node via the median heuristic applied to the observations of X_v (such quantities are available when generating the dictionary), and we define $\sigma_{\min} = \operatorname{argmin}\{\sigma_v\}_{v \in V}$, $\sigma_{\text{median}} = \operatorname{median}\{\sigma_v\}_{v \in V}$ and $\sigma_{\max} = \operatorname{argmax}\{\sigma_v\}_{v \in V}$, we then chose the final parameter from the set $\{\sigma_{\min}, \frac{1}{2}(\sigma_{\min} + \sigma_{\text{median}}), \sigma_{\text{median}}, \frac{1}{2}(\sigma_{\max} + \sigma_{\text{median}}), \sigma_{\max}\}$. γ is selected from the set $\{1e^{-5}, 1e^{-3}, 0.1, 1\}$. Finally, we define the average node degree \bar{d} , and we identify the optimal λ^* from the set $\{1e^{-3} \cdot \frac{1}{\bar{d}}, 1e^{-2} \cdot \frac{1}{\bar{d}}, 0.1 \cdot \frac{1}{\bar{d}}, 1 \cdot \frac{1}{\bar{d}}, 10 \cdot \frac{1}{\bar{d}}\}$.

4.1 Use-cases on synthetic data

In this section, we present two different synthetic scenarios to test the performance of OCKG with different kinds of change-points and graph structures. Two extra scenarios are included in the Appendix.

The graph structures that we analyze are the Stochastic Block Models (Holland et al., 1983) and the Barabási–Albert Model (Albert and Barabási, 2002). In order to keep the simulation results comparable between random instances. We generate a fixed instance for each graph model and over it 50 instances of each of the synthetic scenarios described below:

I. Changes in node clusters. We sample a Stochastic Block Model with 4 clusters, C_1, \dots, C_4 , each containing 20 nodes. The intra- and inter-cluster node connection probability is fixed at 0.5 and 0.01, respectively.

Bivariate Gaussian distribution to Gaussian copula with uniform marginals. In this first experiment, all nodes will follow a bivariate Gaussian model with the same covariance matrix and mean vector. Then we pick a cluster C at time $t = 2000$. From this moment, nodes of C will generate observations from a Gaussian copula ($\sim GC$) whose marginals follow uniform distributions ($\sim U(-c, c)$):

$$\begin{aligned} (x, y) &\sim N(\mu, \Sigma), \quad \mu = (0, 0), \quad \Sigma_{x,x} = 1, \Sigma_{x,y} = \frac{4}{5} \rightarrow \\ (x, y) &\sim GC, \quad \Sigma_{x,x} = 1, \Sigma_{x,y} = \frac{4}{5}. \end{aligned} \quad (16)$$

The parameter c is chosen so the mean vector and covariance matrix before and after the change-point are the same. This particular example is hard as the probabilistic model do not depend on the same set of parameters and the first two moments which are used for basic non-parametric methods are the same.

II. Changes in a subset of connected nodes. We generate a Barabási–Albert Model with 100 nodes. We start with one node, and then one new node is added at each iteration i and get connected with one of the nodes present at $i - 1$ with a probability proportional to their degree. For each instance of the experiments, we will generate C by selecting a node at random with probability proportional to its degree and all the nodes that are at a distance of 4 in the graph. These nodes will suffer a change in the probability model generating its associated stream.

Shift in the mean on one of the cluster components. The streams observed at each of the components are drawn from a different multivariate Gaussian distribution of dimension 3, before and after the change-point at time $\tau = 1000$:

$$\begin{aligned} x_v &\sim N(\mu, \Sigma), \mu = \mathbf{0}_3, \Sigma_{i,i} = 1, \Sigma_{1,2} = \frac{4}{5}, \Sigma_{3,1} = 0 \rightarrow \\ x_v &\sim N(\mu, \Sigma), \mu = (1, 0, 0), \Sigma_{i,i} = 1, \Sigma_{1,2} = \frac{4}{5}, \Sigma_{3,1} = 0. \end{aligned} \quad (17)$$

Further change-point detection scenarios are explored in the Appendix C

Discussion on the results. The results of the synthetic experiments are summarized in Tab. 1 and Fig. 2. As it was explained before, the method derived from the non-parametric LRE lack a solid theoretical and computationally efficient methodology to fix the parameter related with the detection of the change point, η and η_v . Nevertheless, the related scores are expected to achieve its highest value around $\tau + n$. In order to make fair comparison between methods, we report the expected delay based on the peak observed in the time-series of the global score generated by each method. Similarly, we compare the methods in terms of the averaged ROC curves of the classification problem aiming to detect the set of nodes that are chosen in each synthetic scenario, such curves are based on the node level scores observed at time $\tau + n$. In Tab. 1 we report the averaged AUC of the ROC curves and its standard deviation, as well as the percentage of times when the changepoint τ was successfully identified.

We can see in Tab. 1 and Fig. 2 that the performance of the algorithms improve as the number of observations increases in general, which is not surprising. We can see that the Nougat method requires the largest amount of observations to identify τ and the set C . We believe that is due to the stochastic gradient descent step, which produces more noisy detection scores when compared with other methods. In most synthetic scenarios, OCKG-based variants have the

Scenario: Experiment I	Detector	Detection delay (std)	AUC (std)	Precision	Scenario: Experiment II	Detector	Detection delay (std)	AUC (std)	Precision
$n=125$	OCKG $\alpha=0.1$	126.26 (11.95)	0.89 (0.05)	1.00	$n=25$	OCKG $\alpha=0.1$	25.44 (1.96)	0.97 (0.02)	1.00
	OCKG $\alpha=0.5$	129.67 (11.37)	0.85 (0.06)	0.98		OCKG $\alpha=0.5$	25.06 (1.34)	0.97 (0.02)	0.96
	Pool $\alpha=0.1$	123.72 (24.08)	0.82 (0.05)	0.58		Pool $\alpha=0.1$	24.51 (1.68)	0.91 (0.03)	0.82
	Pool $\alpha=0.5$	131.90 (21.02)	0.80 (0.05)	0.80		Pool $\alpha=0.5$	24.44 (2.03)	0.93 (0.02)	0.86
	Nougat	146.50 (70.74)	0.56 (0.22)	0.12		Nougat	34.25 (13.80)	0.64 (0.17)	0.08
$n=250$	OCKG $\alpha=0.1$	252.72 (14.82)	0.93 (0.03)	1.00	$n=50$	OCKG $\alpha=0.1$	50.38 (1.21)	0.99 (0.01)	1.00
	OCKG $\alpha=0.5$	251.31 (21.82)	0.89 (0.04)	0.98		OCKG $\alpha=0.5$	50.67 (1.48)	0.96 (0.04)	0.98
	Pool $\alpha=0.1$	249.54 (25.20)	0.86 (0.04)	0.92		Pool $\alpha=0.1$	48.55 (5.14)	0.91 (0.04)	0.98
	Pool $\alpha=0.5$	245.32 (22.20)	0.87 (0.04)	0.94		Pool $\alpha=0.5$	49.63 (2.38)	0.99 (0.01)	0.98
	Nougat	273.50 (96.59)	0.67 (0.19)	0.20		Nougat	77.84 (10.24)	0.75 (0.17)	0.76
$n=500$	OCKG $\alpha=0.1$	502.70 (6.49)	0.99 (0.00)	1.00	$n=100$	OCKG $\alpha=0.1$	100.52 (1.25)	0.99 (0.00)	1.00
	OCKG $\alpha=0.5$	500.84 (5.15)	0.99 (0.00)	1.00		OCKG $\alpha=0.5$	100.16 (0.64)	1.00 (0.00)	1.00
	Pool $\alpha=0.1$	506.20 (18.31)	0.99 (0.00)	1.00		Pool $\alpha=0.1$	99.86 (1.23)	0.99 (0.00)	1.00
	Pool $\alpha=0.5$	501.90 (7.86)	0.99 (0.00)	1.00		Pool $\alpha=0.5$	100.38 (1.01)	0.99 (0.00)	1.00
	Nougat	576.86 (129.27)	0.66 (0.20)	0.74		Nougat	127.52 (13.87)	0.77 (0.16)	0.88

Table 1: Performance comparison between change-point detectors in three synthetic scenarios for different window sizes (n value). The mean and standard deviation of the score is based on 50 instances.

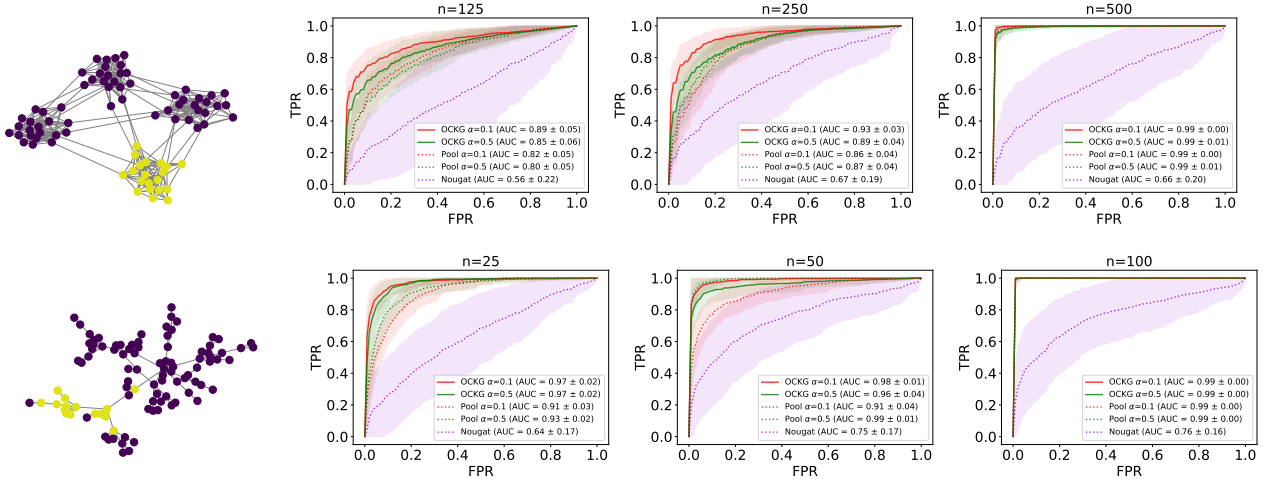


Figure 2: Each row presents results for the two synthetic scenarios. In the first column, an instance of the simulated nodes that suffer a change-point is shown (yellow nodes). The next columns show the mean ROC curves along with their standard deviations for different window sizes n . The mean and standard deviations are estimated based on 50 random instances. – *Experiment I:* A bivariate Gaussian distribution changes to Gaussian copula with uniform marginals. The change affects one cluster of nodes. – *Experiment II:* Change in the mean in one dimension of a 3d Gaussian distribution. The change affects a small set of connected nodes.

best performance in situations where fewer observations are available, as it can be seen in the related precision and AUC scores. Then, by exploiting the graph component, a method enhances the precision of the change-point detection and lowers the detection delay. With respect to the parameter α , the experiments suggest the use of smaller values, such as $\alpha = 0.1$, to keep the detector sensitive to situations in which the Pearson’s Divergence between the pre- and post-change pdfs is expected to be small.

5 Conclusions

In this paper, we introduced a framework to detect change-points in multivariate streams over the nodes of a graph. The main appeal of our approach is its non-parametric formulation that integrates the a priori provided information of the graph structure, and is able to spot different types of

change-point with minimum hypotheses.

In the experiments, we provided evidence showing how the Laplacian regularization leads to an online detector with a lower expected detection time. Moreover, this compares nicely against other alternatives, such as the Nougat method, which also exploits the graph structure. Moreover, the formulation of the cost function based on the Pearson’s Divergence leads to an elegant optimization problem with convenient convergence guarantees.

There are still some questions that remain to be answered and can be part of future work: the selection of the threshold parameters, which is an open problem in general for non-parametric likelihood-ratio based methods, and requires a broader theoretical analysis; the time-dependency of the data; and cases where there is a delay in how each node reacts to a change-point.

6 Acknowledgments

This work was supported by the Industrial Data Analytics and Machine Learning (IdAML) Chair hosted at ENS Paris-Saclay, University Paris-Saclay, and grants from Région Ile-de-France.

References

- Albert, R. and Barabási, A.-L. (2002). Statistical mechanics of complex networks. *Rev. Mod. Phys.*, 74:47–97.
- Aminikhanghahi, S. and Cook, D. J. (2017). Using change point detection to automate daily activity segmentation. In *IEEE Int. Conf. on Pervasive Computing and Communications Workshops*, pages 262–267.
- Arlot, S., Celisse, A., and Harchaoui, Z. (2019). A kernel multiple change-point algorithm via model selection. *Journal of Machine Learning Research*, 20(162):1–56.
- Beck, A. and Tetrushvili, L. (2013). On the convergence of block coordinate descent type methods. *SIAM Journal on Optimization*, 23:2037–2060.
- Bouchikhi, I., Ferrari, A., Richard, C., Bourrier, A., and Bernot, M. (2019). Kernel based online change point detection. In *European Signal Processing Conf.*, pages 1–5.
- Csiszár, I. (1967). On topological properties of f -divergences. *Studia Scientiarum Mathematicarum Hungarica*, 2:329–339.
- de la Concha, A., Kalogeratos, A., and Vayatis, N. (2022). Collaborative likelihood-ratio estimation over graphs.
- Ferrari, A. and Richard, C. (2020). Non-parametric community change-points detection in streaming graph signals. In *IEEE Int. Conf. on Acoustics, Speech and Signal Processing*, pages 5545–5549.
- Ferrari, A., Richard, C., Bourrier, A., and Bouchikhi, I. (2021). Online change-point detection with kernels.
- Harchaoui, Z., Moulines, E., and Bach, F. (2008). Kernel change-point analysis. In Koller, D., Schuurmans, D., Bengio, Y., and Bottou, L., editors, *Advances in Neural Information Processing Systems*, volume 21. Curran Associates, Inc.
- Holland, P. W., Laskey, K. B., and Leinhardt, S. (1983). Stochastic blockmodels: First steps. *Social Networks*, 5(2):109–137.
- Kanamori, T., Suzuki, T., and Sugiyama, M. (2012). f -divergence estimation and two-sample homogeneity test under semiparametric density-ratio models. *IEEE Trans. on Information Theory*, 58(2):708–720.
- Kawahara, Y. and Sugiyama, M. (2012). Sequential change-point detection based on direct density-ratio estimation. *Statistical Analysis and Data Mining: The ASA Data Science Journal*, 5(2):114–127.
- Kullback, S. (1959). *Information Theory and Statistics*. Wiley.
- Li, S., Xie, Y., Dai, H., and Song, L. (2019). Scan B-statistic for kernel change-point detection. *Sequential Analysis*, 38(4):503–544.
- Li, X., Zhao, T., Arora, R., Liu, H., and Hong, M. (2018). On faster convergence of cyclic block coordinate descent-type methods for strongly convex minimization. *Journal of Machine Learning Research*, 18(184):1–24.
- Nguyen, X., Wainwright, M. J., and Jordan, M. (2008). Estimating divergence functionals and the likelihood ratio by penalized convex risk minimization. In *Advances in Neural Information Processing Systems*.
- Page, E. S. (1954). Continuous inspection schemes. *Biometrika*, 41(1–2):100–115.
- Pearson, K. (1900). X. On the criterion that a given system of deviations from the probable in the case of a correlated system of variables is such that it can be reasonably supposed to have arisen from random sampling. *The London, Edinburgh, and Dublin Philosophical Magazine and Journal of Science*, 50(302):157–175.
- Richard, C., Bermudez, J. C. M., and Honeine, P. (2009). Online prediction of time series data with kernels. *IEEE Trans. on Signal Processing*, 57(3):1058–1067.
- Sharpnack, J., Rinaldo, A., and Singh, A. (2016). Detecting anomalous activity on networks with the graph fourier scan statistic. *IEEE Trans. on Signal Processing*, 64(2):364–379.
- Sheldon, D. (2008). Graphical Multi-Task Learning. Technical report, Cornell University.
- Shewhart, W. A. (1925). The application of statistics as an aid in maintaining quality of a manufactured product. *Journal of the American Statistical Association*, 20(152):546–548.
- Shiryayev, A. N. (1963). On optimum methods in quickest detection problems. *Theory of Probability & Its Applications*, 8(1):22–46.
- Shuman, D. I., Narang, S. K., Frossard, P., Ortega, A., and Vandergheynst, P. (2013). The emerging field of signal processing on graphs: Extending high-dimensional data analysis to networks and other irregular domains. *IEEE Signal Processing Magazine*, 30(3):83–98.
- Sugiyama, M., Nakajima, S., Kashima, H., Buenau, P., and Kawanabe, M. (2007). Direct importance estimation with model selection and its application to covariate shift adaptation. In *Advances in Neural Information Processing Systems*.
- Sugiyama, M., Suzuki, T., Itoh, Y., Kanamori, T., and Kimura, M. (2011). Least-squares two-sample test. *Neural networks*, 24:735–51.

- Tartakovsky, A. (2021). *Sequential change detection and hypothesis testing : general non-i.i.d. stochastic models and asymptotically optimal rules*. Chapman & Hall/CRC.
- Tartakovsky, A., Nikiforov, I., and Basseville, M. (2014). *Sequential Analysis: Hypothesis Testing and Change-point Detection*. Chapman & Hall/CRC Monographs on Statistics & Applied Probability. Taylor & Francis, CRC Press.
- Xie, L., Zou, S., Xie, Y., and Veeravalli, V. V. (2021). Sequential (quickest) change detection: Classical results and new directions. *IEEE Journal on Selected Areas in Information Theory*.
- Yamada, M., Suzuki, T., Kanamori, T., Hachiya, H., and Sugiyama, M. (2011). Relative density-ratio estimation for robust distribution comparison. In *Advances in Neural Information Processing Systems*.
- Zou, S. and Veeravalli, V. V. (2018). Quickest detection of dynamic events in sensor networks. In *IEEE Int. Conf. on Acoustics, Speech and Signal Processing*, pages 6907–6911.
- Zou, S., Veeravalli, V. V., Li, J., Towsley, D., and Swami, A. (2019). Distributed quickest detection of significant events in networks. In *IEEE Int. Conf. on Acoustics, Speech and Signal Processing*, pages 8454–8458.

APPENDIX

A Analysis of the proposed optimization algorithm

In this section, we discuss the details of the Cyclic Block Gradient Descent strategy described in Sec. 3.3. In particular, we are interested in proving an upper bound for the number of interactions to attain a given precision ϵ in terms of the size of the dictionary and the number of nodes. We use $e_{\max}(A)$ to indicate the maximum eigenvalue of the square matrix A .

Theorem 1. *Suppose that for a dictionary D of size $L \geq 2$ we aim to solve the Optimization Problem 10 via the Cyclic Block Gradient Descent strategy, where the update with respect to the node parameter θ_v at the i -th cycle is computed by:*

$$\begin{aligned} \hat{\theta}_{v,t}^{(i)} = & \frac{\eta_{v,t}}{\eta_{v,t} + \lambda\gamma} \hat{\theta}_{v,t}^{(i-1)} - \frac{1}{\eta_{v,t} + \lambda\gamma} \left[\left(\frac{(1-\alpha)H_{v,t} + \alpha H'_{v,t}}{N} \right) \hat{\theta}_{v,t}^{(i-1)} - \frac{h'_{v,t}}{N} \right] \\ & - \frac{\lambda}{\eta_{v,t} + \lambda\gamma} \left[d_v \hat{\theta}_{v,t}^{(i-1)} - \sum_{u \in \text{ng}(v)} W_{uv} (\hat{\theta}_{u,t}^{(i)} \mathbf{1}_{u < v} + \hat{\theta}_{u,t}^{(i-1)} \mathbf{1}_{u \geq v}) \right]. \end{aligned} \quad (18)$$

Then, if we fix the learning rate for node v at $\eta_{v,t} = e_{\max} \left(\frac{(1-\alpha)}{N} H_{v,t} + \frac{\alpha}{N} H'_{v,t} + \lambda d_v \mathbb{I}_L \right)$, we will need at most the following number of interactions in order to achieve a pre-specified accuracy level $\epsilon > 0$:

$$i_{\max} = \left\lceil \frac{\lambda\gamma(M_{\min} + \lambda\gamma) + 16M^2 \log^2(3NL)}{\lambda\gamma(M_{\min} + \lambda\gamma)} \log \left(\frac{\Phi(\Theta_t^{(0)}) - \Phi(\Theta_t^*)}{\epsilon} \right) \right\rceil, \quad (19)$$

where:

$$\Phi(\Theta) = \frac{1}{N} \sum_{v \in V} \ell_{v,t}(\theta_v) + \frac{\lambda}{2} \Theta^\top ([\mathcal{L} + \gamma \mathbb{I}_N] \otimes \mathbb{I}_L) \Theta \quad (20)$$

$$M = e_{\max} \left(\frac{1-\alpha}{N} H_t + \frac{\alpha}{N} H'_t + \lambda[\mathcal{L} \otimes \mathbb{I}_L] \right), \quad M_v = e_{\max} \left(\frac{(1-\alpha)}{N} H_{v,t} + \frac{\alpha}{N} H'_{v,t} + \lambda d_v \mathbb{I}_L \right), \quad M_{\min} = \min_{v \in V} M_v. \quad (21)$$

Theorem 1 is a particular case of the results appearing in the paper Li et al. (2018). In that work, the authors analyzed the convergence Cyclic Block Coordinate type-algorithms. For completeness of the presentation, we present some of their main results.

The objective functions analyzed in Li et al. (2018) take the form:

$$\min_{\Theta \in \mathbb{R}^M} \Phi(\Theta) = \min_{\theta \in \mathbb{R}^M} Q(\Theta) + R(\Theta), \quad (22)$$

where Q is a twice differentiable loss function, R is a possibly non-smooth and strongly convex penalty function and the variable Θ is of dimension $L = \sum_{v=1}^N L_v$ and is partitioned into disjoint blocks, $\Theta = (\theta_1, \theta_2, \dots, \theta_N)$, each of them being of dimension M_v . It is supposed the penalization term can be written as $R(\Theta) = \sum_{v=1}^N R_v(\theta_v)$.

Assumption A. 1. $Q(\cdot)$ is convex, and its gradient mapping $\Delta Q(\cdot)$ is Lipschitz-continuous and also block-wise Lipschitz-continuous, i.e. there exist positive constants M and M_v such that for any $\Theta, \Theta' \in \mathbb{R}^M$ and $v = 1, \dots, N$, we have:

$$\begin{aligned} \|\Delta Q(\Theta') - \Delta Q(\Theta)\| & \leq M \|\Theta' - \Theta\| \\ \|\Delta_v Q(\theta'_{u < v}, \theta_v, \theta'_{u > v}) - \Delta_v Q(\theta')\| & \leq M_v \|\theta_v - \theta'_v\|. \end{aligned} \quad (23)$$

Assumption A. 2. $R(\cdot)$ is strongly convex and also block-wise strongly convex, i.e. there exist positive constants μ and μ'_v s such that for any $\Theta, \Theta' \in \mathbb{R}^M$ and $v \in V$, we have:

$$\begin{aligned} R(\Theta) & \geq R(\Theta') + (\Theta - \Theta')^\top \xi + \frac{\mu}{2} \|\Theta - \Theta'\|^2, \\ R_v(\theta_v) & \geq R_v(\theta'_v) + (\theta_v - \theta'_v)^\top \xi_v + \frac{\mu_v}{2} \|\theta_v - \theta'_v\|^2, \end{aligned} \quad (24)$$

for all $\xi \in \Delta R(\Theta')$.

Under the aforementioned hypothesis, the Cyclic Block Gradient Descent method, in which the cycle i for block v , is defined as:

$$\hat{\theta}_v^{(i)} = \operatorname{argmin}_{\theta_v} (\theta_v - \hat{\theta}_v^{(i-1)})^T \Delta_v Q(\hat{\theta}_{u < v}^{(i)}, \hat{\theta}_{u \geq v}^{(i-1)}) + \frac{\eta_v}{2} \left\| \theta_v - \hat{\theta}_v^{(i-1)} \right\|^2 + R_v(\theta_v). \quad (25)$$

Then, Theorem A.1 characterizes the maximum number of interaction required to achieve a pre-specified accuracy ϵ .

Theorem A. 1. (Theorem 3 in Li et al. (2018)) – Suppose that Assumptions 1 and 2 hold with $L \geq 2$. And that the optimization point is Θ^* . We choose $\alpha_v = M_v$ for the CBC method. Given a pre-specified accuracy $\epsilon > 0$ of the objective value, we need at most

$$i_{\max} = \left\lceil \frac{\mu M_{\min}^\mu + 16M^2 \log^2(3NL_{\max})}{\mu M_{\min}^\mu} \log\left(\frac{\phi(\Theta^{(0)}) - \phi(\Theta^*)}{\epsilon}\right) \right\rceil \quad (26)$$

iterations to ensure $\phi(\Theta^{(i)}) - \phi(\Theta^*) < \epsilon$ for $i \geq i_{\max}$, where $M_{\min}^\mu = \min_{v \in V} M_v + \mu_v$ and $L_{\max} = \max_{v \in V} L_v$.

Proof of Theorem 1.

Proof. Given that all the parameters θ_v are of dimension L , that is the dimension of the dictionary D , and we have N nodes, then the total dimension of the parameter Θ is LN .

To facilitate the comparison of Problem 10 and the formulation Expr. 22, we recall the terms:

$$h'_t = (h'_{1,t}, \dots, h'_{N,t}) \in \mathbb{R}^{NL}, \quad H' = \operatorname{Block}(H'_{1,t}, \dots, H'_{N,t}) \in \mathbb{R}^{LN \times LN}, \quad H = \operatorname{Block}(H_{1,t}, \dots, H_{N,t}) \in \mathbb{R}^{LN \times LN} \quad (27)$$

Then, we identify the functions Q and R as:

$$\begin{aligned} Q(\Theta) &= \frac{1}{N} \left((1-\alpha) \frac{\Theta^T H_t \Theta}{2} + \alpha \frac{\Theta^T H'_t \Theta}{2} - h'_t{}^T \Theta \right) + \frac{\lambda}{2} \Theta^T (\mathcal{L} \otimes \mathbb{I}_L) \Theta \\ &= \frac{1}{N} \sum_{v \in V} \left((1-\alpha) \frac{\theta_v^T H_{v,t} \theta_v}{2} + \alpha \frac{\theta_v^T H'_{v,t} \theta_v}{2} - h'_{v,t}{}^T \theta_v \right) + \frac{\lambda}{4} \sum_{u,v \in V} W_{uv} \|\theta_u - \theta_v\|^2, \\ R(\theta) &= \frac{\lambda\gamma}{2} \sum_{v \in V} R_v(\theta_v) = \frac{\lambda\gamma}{2} \sum_{v \in V} \|\theta_v\|^2. \end{aligned} \quad (28)$$

Given this notation, it is easy to verify that updating scheme of Eq. 25 takes the form of Eq. 18.

It is clear that, by definition, that $R(\Theta)$ and $R_v(\theta_v)$ are stronger convex functions of modulus $\lambda\gamma$. Then Assumption 2 is satisfied.

Second, the full gradient of $Q(\cdot)$ can be written as:

$$\Delta Q(\Theta) = \left(\frac{1-\alpha}{N} H_t + \frac{\alpha}{N} H'_t + \lambda(\mathcal{L} \otimes \mathbb{I}_L) \right) \Theta - \frac{1}{N} h'_t, \quad (29)$$

which is Lipschitz-continuous with constant $M = e_{\max} \left(\frac{1-\alpha}{N} H_t + \frac{\alpha}{N} H'_t + \lambda(\mathcal{L} \otimes \mathbb{I}_L) \right)$. From the node-level expression is easy to derive the partial derivative of $Q(\cdot)$:

$$\Delta_{\theta_v} Q(\Theta) = \left(\frac{(1-\alpha)H_{v,t} + \alpha H'_{v,t}}{N} \right) \theta_v + \lambda \left(d_v \theta_v - \sum_{u \in \operatorname{ng}(v)} W_{uv} (\theta_u \mathbf{1}_{u < v} + \theta_u \mathbf{1}_{u > v}) \right) - \frac{h'_{v,t}}{N}, \quad (30)$$

where d_v is the degree of node v . This means:

$$\|\Delta_v Q(\theta'_{u < v}, \theta_v, \theta'_{u > v}) - \Delta_v Q(\Theta')\| \leq \left\| \left(\frac{(1-\alpha)H_{v,t} + \alpha H'_{v,t}}{N} + \lambda d_v \mathbb{I}_L \right) (\theta_v - \theta'_v) \right\| \leq M_v \|\theta_v - \theta'_v\|, \quad (31)$$

where $M_v = e_{\max} \left(\frac{(1-\alpha)H_{v,t} + \alpha H'_{v,t}}{N} + \lambda d_v \mathbb{I}_L \right)$.

Then, Assumption 1 is satisfied.

With these elements, and by fixing $\eta_v = M_v$, we can apply Theorem A.1 where

$$M = e_{\max} \left(\frac{1-\alpha}{N} H_t + \frac{\alpha}{N} H'_t + \lambda(\mathcal{L} \otimes \mathbb{I}_L) \right), \quad M_v = e_{\max} \left(\frac{(1-\alpha)H_{v,t} + \alpha H'_{v,t}}{N} + \lambda d_v \mathbb{I}_L \right), \quad M_{\min}^{\mu} = \min_{v \in V} M_v + \mu \quad (32)$$

$$\mu = \lambda \gamma.$$

After substitution, we get the expression given in Eq. 19. \square

B Hyperparameter selection strategy

In this section, we detail the model selection strategy to identify the best hyperparameters including the hyperparameters of the Kernel and the penalization constants γ, λ . To make it easier to be read, we denote by σ the hyperparameters associated with the Kernel of interest. The full framework is written in Alg. 2.

Algorithm 2 – Hyperparameters tuning for OCKG

- 1: **Input:** $\mathcal{X}, \mathcal{X}'$: the adjacent set of observations to be used for estimating the relative likelihood-ratios:
 $\mathcal{X} := [\mathcal{X}_1, \dots, \mathcal{X}_N] = [[x_{1,1}, \dots, x_{1,n}], \dots, [x_{N,1}, \dots, x_{N,n}]]$
 $\mathcal{X}' := [\mathcal{X}'_1, \dots, \mathcal{X}'_N] = [[x'_{1,1}, \dots, x'_{1,n}], \dots, [x'_{N,1}, \dots, x'_{N,n}]]$
 $\mathcal{G} = (V, E)$: Observed graph structure;
 D : a precomputed dictionary, associated with the chosen kernel, containing L elements;
 Σ, Λ, Γ : parameter grid of parameters to explore for σ, λ, γ ;
 R : the number of random splits.
 - 2: **Output:** σ^* the optimal parameter for the kernel K , and the two penalization constants λ^* and γ^* .
-

- 3: Randomly split $\{1, \dots, n\}$ into R disjoint subsets $\{I_r\}_{r \in \{1, \dots, R\}}$. Define the subsamples:

$$\mathcal{X}_r = [\mathcal{X}_{1,r}, \dots, \mathcal{X}_{N,r}] = [[x_{1,i}, i \in I_r], \dots, [x_{N,i}, i \in I_r]]$$

$$\mathcal{X}'_r = [\mathcal{X}'_{1,r}, \dots, \mathcal{X}'_{N,r}] = [[x'_{1,i}, i \in I_r], \dots, [x'_{N,i}, i \in I_r]]$$

- 4: **for** each $\sigma \in \Sigma$ **do**
 - 5: **for** each $(\lambda, \gamma) \in \Lambda \times \Gamma$ **do**
 - 6: **for** each data subset $r = 1, \dots, R$ **do**
 - 7: Let $\mathcal{X}'_{\text{train}} = \mathcal{X}' \setminus \mathcal{X}'_r$, $\mathcal{X}'_{\text{test}} = \mathcal{X}'_r$, and $\mathcal{X}_{\text{train}} = \mathcal{X} \setminus \mathcal{X}_r$, $\mathcal{X}_{\text{test}} = \mathcal{X}_r$
 - 8: Compute $h'_{v,\text{train}}(\sigma) = \frac{1}{n} \sum_{x \in \mathcal{X}'_{v,\text{train}}} \phi(x, \sigma)$ and $H'_{v,\text{train}}(\sigma) = \frac{1}{n} \sum_{x \in \mathcal{X}'_{v,\text{train}}} \phi(x, \sigma) \phi(x, \sigma)^T$
 - 9: Compute $H_{v,\text{train}}(\sigma) = \frac{1}{n} \sum_{x \in \mathcal{X}_{v,\text{train}}} \phi(x, \sigma) \phi(x, \sigma)^T$.
 - 10: Solve

$$\hat{\Theta}(\gamma, \lambda) = \underset{\Theta}{\operatorname{argmin}} \frac{1}{N} \sum_{v \in V} \ell_v(\theta_v) + \frac{\lambda}{2} \Theta^T ([\mathcal{L} + \gamma \mathbb{I}_N] \otimes \mathbb{I}_L) \Theta$$

where

$$\ell_v(\theta_v) = (1-\alpha) \frac{\theta_v^T H_{v,\text{train}} \theta_v}{2} + \alpha \frac{\theta_v^T H'_{v,\text{train}} \theta_v}{2} - h'_{v,\text{train}} \theta_v$$
 - 11: Compute $h'_{v,\text{test}}(\sigma) = \frac{1}{n} \sum_{x \in \mathcal{X}'_{v,\text{test}}} \phi(x, \sigma)$ and $H'_{v,\text{test}}(\sigma) = \frac{1}{n} \sum_{x \in \mathcal{X}'_{v,\text{test}}} \phi(x, \sigma) \phi(x, \sigma)^T$
 - 12: Compute $H_{v,\text{test}}(\sigma) = \frac{1}{n} \sum_{x \in \mathcal{X}_{v,\text{test}}} \phi(x, \sigma) \phi(x, \sigma)^T$.
 - 13: Compute

$$\ell^{(r)}(\hat{\Theta}(\gamma, \lambda)) = \frac{1}{N} \sum_{v \in V} (1-\alpha) \frac{\hat{\theta}_v^T H_{v,\text{test}} \hat{\theta}_v}{2} + \alpha \frac{\hat{\theta}_v^T H'_{v,\text{test}} \hat{\theta}_v}{2} - h'_{v,\text{test}} \hat{\theta}_v$$
 - 14: **end for**
 - 15: Compute $\hat{\ell}(\sigma, \lambda, \gamma) = \frac{1}{R} \sum_{r=1}^R \ell^{(r)}(\Theta)$
 - 16: **end for**
 - 17: **end for**
 - 18: **return** $\sigma^*, \lambda^*, \gamma^* = \operatorname{argmin}_{\sigma, \lambda, \gamma} \hat{\ell}(\sigma, \lambda, \gamma)$
-

C Further experiments

In order to enhance comprehension, we present the complete experimental setting, by including also the two experiments described in the main text. The implementation details of the four scenarios remains the same as what described in Sec. 4.

I. Changes in node clusters. We sample a Stochastic Block Model with 4 clusters, C_1, \dots, C_4 , each containing 20 nodes. The intra- and inter-cluster node connection probability is fixed at 0.5 and 0.01, respectively.

I.a. Bivariate Gaussian distribution to Gaussian copula with uniform marginals.

In this first experiment, all nodes will follow a bivariate Gaussian model with the same covariance matrix and mean vector. Then we pick a cluster C at time $t = 2000$. From this moment, nodes of C will generate observations from a Gaussian copula ($\sim GC$) whose marginals follow uniform distributions ($\sim U(-c, c)$):

$$(x, y) \sim N(\mu, \Sigma), \mu = (0, 0), \Sigma_{x,x} = 1, \Sigma_{x,y} = \frac{4}{5} \rightarrow (x, y) \sim GC, \Sigma_{x,x} = 1, \Sigma_{x,y} = \frac{4}{5}. \quad (33)$$

The parameter c is chosen so the mean vector and covariance matrix before and after the change-point are the same. This particular example is hard as the probabilistic model do not depend on the same set of parameters and the first two moments which are used for basic non-parametric methods are the same.

I.b. Change in the covariance matrix or mean vector of bivariate Gaussian distribution. The observations at each node follow a bivariate Gaussian distribution whose parameters μ and Σ depend on the cluster they belong to. All of them have variance 1 in both dimensions. We select two cluster of nodes at random and inject a change-point according to the following schema:

$$\begin{cases} \mu = (0, 0), \Sigma_{1,2} = \frac{4}{5} & \rightarrow \mu = (0, 0), \Sigma_{1,2} = \frac{-4}{5} & \text{if } C1 \\ \mu = (0, 0), \Sigma_{1,2} = \frac{4}{5} & \rightarrow \mu = (0, 0), \Sigma_{1,2} = 0 & \text{if } C2 \\ \mu = (0, 0), \Sigma_{1,2} = \frac{-4}{5} & \rightarrow \mu = (0, 0), \Sigma_{1,2} = 0 & \text{if } C3 \\ \mu = (0, 0), \Sigma_{1,2} = \frac{4}{5} & \rightarrow \mu = (1, 1), \Sigma_{1,2} = \frac{4}{5} & \text{if } C4. \end{cases} \quad (34)$$

The set of observations is of length 1000 and the change-point is observed at time 500. Notice that the difficulty of the detection task will depend on the selected clusters.

II. Changes in set of connected nodes. In this set of experiments, we sample a Barabási-Albert model with 100 nodes. This generative model will start with a node at the first iteration, then a node will appear at each iteration i and connect with one of the nodes present at $i - 1$ with a probability proportional to their degrees.

For each instance of the experiments, we will generate C by selecting a node at random with probability proportional to its degree and all the nodes that are at a distance of 4 in the graph. These nodes will suffer a change in the probability model generating its associated stream. These transitions are described bellow:

II.a. Shift in the mean on one of the cluster components. The streams observed at each of the components are drawn from a different 3d Gaussian distribution, before and after the change-point at time $\tau = 1000$:

$$x_v \sim N(\mu, \Sigma), \mu = \mathbf{0}_3, \Sigma_{i,i} = 1, \Sigma_{1,2} = \frac{4}{5}, \Sigma_{3,1} = 0 \rightarrow x_v \sim N(\mu, \Sigma), \mu = (1, 0, 0), \Sigma_{i,i} = 1, \Sigma_{1,2} = \frac{4}{5}, \Sigma_{3,1} = 0. \quad (35)$$

II.b. Change in probability law. All the nodes will generate observations from standard normal distributions. Then, at time $\tau = 2000$, nodes who are in C will start to follow a centralized uniform distributions with unit variance:

$$x_v \sim N(0, 1) \rightarrow x_v \sim U(-\sqrt{3}, \sqrt{3}) \text{ if } v \in C. \quad (36)$$

Scenario	Detector	Detection		
		delay (std)	AUC (std)	Precision
Experiment I.A $n=125$	OCKG $\alpha = 0.1$	126.26 (11.95)	0.89 (0.05)	1.00
	OCKG $\alpha = 0.5$	129.67 (11.37)	0.85 (0.06)	0.98
	Pool $\alpha = 0.1$	123.72 (24.08)	0.82 (0.05)	0.58
	Pool $\alpha = 0.5$	131.90 (21.02)	0.80 (0.05)	0.80
	Nougat	146.50 (70.74)	0.56 (0.22)	0.12
Experiment I.A $n=250$	OCKG $\alpha = 0.1$	252.72 (14.82)	0.93 (0.03)	1.00
	OCKG $\alpha = 0.5$	251.31 (21.82)	0.89 (0.04)	0.98
	Pool $\alpha = 0.1$	249.54 (25.20)	0.86 (0.04)	0.92
	Pool $\alpha = 0.5$	245.32 (22.20)	0.87 (0.04)	0.94
	Nougat	273.50 (96.59)	0.67 (0.19)	0.20
Experiment I.A $n = 500$	OCKG $\alpha = 0.1$	502.70 (6.49)	0.99 (0.00)	1.00
	OCKG $\alpha = 0.5$	500.84 (5.15)	0.99 (0.00)	1.00
	Pool $\alpha = 0.1$	506.20 (18.31)	0.99 (0.00)	1.00
	Pool $\alpha = 0.5$	501.90 (7.86)	0.99 (0.00)	1.00
	Nougat	576.86 (129.27)	0.66 (0.20)	0.74
Experiment I.B $n=25$	OCKG $\alpha = 0.1$	25.04 (0.20)	0.99 (0.02)	1.00
	OCKG $\alpha = 0.5$	25.06 (0.31)	0.98 (0.02)	1.00
	Pool $\alpha = 0.1$	25.12 (0.48)	0.91 (0.05)	1.00
	Pool $\alpha = 0.5$	25.02 (0.24)	0.96 (0.03)	1.00
	Nougat	40.68 (4.12)	0.76 (0.17)	1.00
Experiment I.B $n = 50$	OCKG $\alpha = 0.1$	50.18 (0.55)	1.00 (0.00)	1.00
	OCKG $\alpha = 0.5$	50.16 (0.54)	0.99 (0.01)	1.00
	Pool $\alpha = 0.1$	50.02 (0.32)	0.93 (0.06)	1.00
	Pool $\alpha = 0.5$	50.00 (0.20)	1.00 (0.00)	1.00
	Nougat	67.98 (7.63)	0.78 (0.17)	0.92
Experiment I.B $n=100$	OCKG $\alpha = 0.1$	100.12 (0.47)	1.00 (0.00)	1.00
	OCKG $\alpha = 0.5$	100.02 (0.14)	1.00 (0.00)	1.00
	Pool $\alpha = 0.1$	100.06 (0.24)	1.00 (0.01)	1.00
	Pool $\alpha = 0.5$	100.00 (0.00)	1.00 (0.00)	1.00
	Nougat	124.23 (13.50)	0.88 (0.09)	1.00
Experiment II.A $n=25$	OCKG $\alpha = 0.1$	25.44 (1.96)	0.97 (0.02)	1.00
	OCKG $\alpha = 0.5$	25.06 (1.34)	0.97 (0.02)	0.96
	Pool $\alpha = 0.1$	24.51 (1.68)	0.91 (0.03)	0.82
	Pool $\alpha = 0.5$	24.44 (2.03)	0.93 (0.02)	0.86
	Nougat	34.25 (13.80)	0.64 (0.17)	0.08
Experiment II.A $n=50$	OCKG $\alpha = 0.1$	50.38 (1.21)	0.99 (0.01)	1.00
	OCKG $\alpha = 0.5$	50.67 (1.48)	0.96 (0.04)	0.98
	Pool $\alpha = 0.1$	48.55 (5.14)	0.91 (0.04)	0.98
	Pool $\alpha = 0.5$	49.63 (2.38)	0.99 (0.01)	0.98
	Nougat	77.84 (10.24)	0.75 (0.17)	0.76
Experiment II.A $n=100$	OCKG $\alpha = 0.1$	100.52 (1.25)	0.99 (0.00)	1.00
	OCKG $\alpha = 0.5$	100.16 (0.64)	1.00 (0.00)	1.00
	Pool $\alpha = 0.1$	99.86 (1.23)	0.99 (0.00)	1.00
	Pool $\alpha = 0.5$	100.38 (1.01)	0.99 (0.00)	1.00
	Nougat	127.52 (13.87)	0.77 (0.16)	0.88
Experiment II.B $n=125$	OCKG $\alpha = 0.1$	128.17 (9.91)	0.86 (0.04)	0.94
	OCKG $\alpha = 0.5$	129.63 (16.66)	0.86 (0.04)	0.96
	Pool $\alpha = 0.1$	130.05 (12.48)	0.79 (0.06)	0.88
	Pool $\alpha = 0.5$	133.64 (15.57)	0.85 (0.05)	0.96
	Nougat	146.08 (17.78)	0.54 (0.19)	0.26
Experiment II.B $n=250$	OCKG $\alpha = 0.1$	249.96 (20.19)	0.96 (0.02)	1.00
	OCKG $\alpha = 0.5$	251.12 (15.29)	0.88 (0.04)	1.00
	Pool $\alpha = 0.1$	258.51 (12.18)	0.92 (0.03)	0.98
	Pool $\alpha = 0.5$	254.58 (19.09)	0.88 (0.04)	1.00
	Nougat	331.00 (121.15)	0.49 (0.17)	0.34
Experiment II.B $n=500$	OCKG $\alpha = 0.1$	498.70 (8.88)	1.00 (0.00)	1.00
	OCKG $\alpha = 0.5$	500.00 (1.80)	1.00 (0.00)	1.00
	Pool $\alpha = 0.1$	497.94 (15.47)	1.00 (0.00)	1.00
	Pool $\alpha = 0.5$	500.12 (2.28)	1.00 (0.00)	1.00
	Nougat	529.86 (68.53)	0.39 (0.16)	0.98

Table 2: Performance comparison between change-point detectors in several synthetic scenarios for different window sizes (n value). The mean and standard deviation of the score is based on 50 instances.

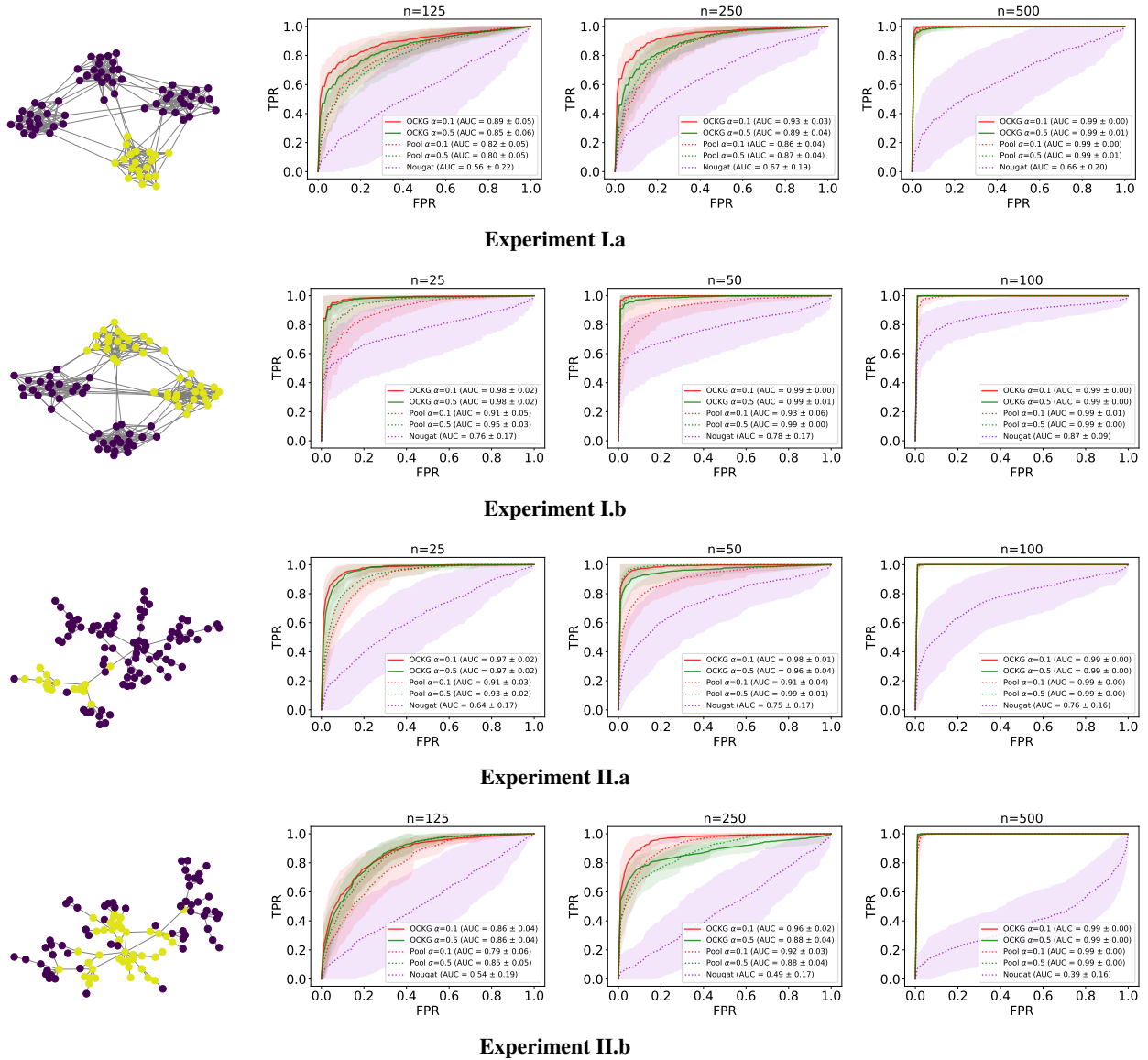


Figure 3: Each row presents results for one synthetic scenario. In the first column, an instance of the simulated nodes that suffer a change-point is shown (yellow nodes). The next columns show the mean ROC curves along with their standard deviations for different window sizes n . The mean and standard deviations are estimated based on 50 random instances. – *Experiment I.a:* A bivariate Gaussian distribution changes to a Gaussian copula with uniform marginals. The change affects one cluster of nodes. – *Experiment I.b:* Change in the covariance matrix or mean vector of bivariate Gaussian distribution. The change affects two clusters of nodes. – *Experiment II.a:* Change in the mean in one dimension of a 3d Gaussian distribution. The change affects a large set of connected nodes. – *Experiment II.b:* A standardized normal distribution changes to a uniform distribution with the same first two second moments. The change affects a small set of connected nodes.